A Fokker-Planck-based numerical method for modelling non-homogeneous flows of dilute polymeric solutions.

Alexei Lozinski [1], Robert G. Owens [2]

LMF - ISE - FSTI, Ecole Polytechnique Fédérale de Lausanne, CH 1015 Lausanne, Switzerland.

Jiannong Fang

GEOLEP-ICARE-ENAC, Ecole Polytechnique Fédérale de Lausanne, CH 1015 Lausanne, Switzerland

Abstract

An original mixed finite-difference/spectral method based upon a Fokker-Planck equation is proposed for the numerical simulation of non-homogeneous flows of FENE-type fluids. Since the configuration distribution function ψ varies as a function of time and in both physical and configuration space careful attention has been paid to the discretization scheme for derivatives of ψ in these variables, the domains of definition of the physical and configuration coordinates being inter-dependent. Numerical results for start-up planar Poiseuille flow are in excellent quantitative agreement with those of a stochastic simulation and, for comparable levels of accuracy, are much less CPU expensive. Theoretical results for the polymeric stress fields under equilibrium conditions are verified numerically and generalize earlier results for Hookean dumbbells by Brunn and Grisafi [P. O. Brunn and S. Grisafi, Chem. Eng. Commun., 36 (1985) 367-383].

Key words: Fokker-Planck equation, non-homogeneous flows, spectral methods

[1] Present address: Chaire d'Analyse et Simulation Numériques, Institut d'Analyse et Calcul Scientifique, Ecole Polytechnique Fédérale de Lausanne, CH 1015 Lausanne, Switzerland.

[2] Author to whom correspondence should be addressed. Email: Robert.Owens@epfl.ch

1 Introduction

Models of polymer solutions based on kinetic theory can usually be described in two formally equivalent ways: via stochastic differential equations or via deterministic Fokker-Planck (FP) equations for the configuration distribution function (cdf). FP-based numerical methods are a competitive alternative to stochastic techniques for the simulation of complex flows of viscoelastic fluids described by dumbbell models or single segment reptation theories, as evidenced in [8,9,19,20]. An important factor in the affordability of the methods described in the cited papers has been the time-splitting employed for the solution of the cdf whereby two half-time steps are performed, corresponding to a solution in configuration space and a solution in physical space (the flow domain). In [8,9] the authors used a spectral method to solve for the cdf of FENE dumbbells in a dilute solution and convincingly demonstrated the huge CPU savings that could be realized over equally accurate simulations using the Brownian configuration fields method [18,27]. In [19] Lozinski and Chauvière introduced for the same model a fast solver based upon a rotation operator applied to all terms in the configuration step and this led to yet greater savings in CPU time relative to stochastic methods. That significant computational savings over stochastic methods could also be achieved for single segment reptation models was evidenced by Lozinski et al. [20] in 2003, where simulations were done using a model due to Öttinger [17,26] for both start-up homogeneous flows as well as flow past a confined cylinder.

A discussion of earlier work by Warner [32] and Fan [12–16] using the FP equation for dumbbell models, mostly for viscometric flows, may be found in the introductory paragraphs of [8] and [20]. Much more recently, the MIT group [1,24,30] has solved the FP equation for multibead-rod models and the Doi model for mono-domain liquid crystalline polymers using a discontinuous Galerkin method in physical space and a Daubechies wavelet basis in configuration space. Given the often highly localized character of the cdf in strong shear and extensional flows its representation in terms of wavelets may be an attractive option in terms of cost and accuracy.

All the papers cited above share a common feature: the fluctuations of the centres of mass of the polymer molecules over particle paths of the solvent are neglected, and this is manifested in the absence of the diffusive term in physical space in the FP equations. Thus, the FP equations used in these papers coincide formally with that developed originally for homogeneous flows (see, for example, [6,28]). The significance of diffusive terms in physical space was underlined for the first time in the literature (to the authors' knowledge) by El-Kareh and Leal in [11]. Although an in-depth assessment of the importance of physical diffusive terms in constitutive models for flows in domains of macroscopic size large compared to molecular length scales is still to be done (but

see a brief discussion in the paragraphs immediately preceding Section 2.1), the diffusive term is certainly non-negligible when the characteristic size of the flow domain is comparable to the molecular size. The present paper, then, is an attempt to use the numerical solution to an appropriate non-homogeneous FP equation to calculate the elastic stress for a FENE dumbbell fluid in such a non-homogeneous flow. We make the usual assumption of equilibration in momentum space when computing the form of the time-smoothed Brownian force and the bead-motion contribution to the Cauchy stress. However, no assumption of constant $\nabla\mathbf{v}$, either globally (homogeneous flow) or even over the length scale of a polymer molecule (local homogeneity), is made.

The presence of a diffusion term in physical space implies the need for the prescription of physical boundary conditions on the cdf, which gives the distribution of the dumbbells' configurations at different points of the fluid. Following Biller and Petruccione [5] we consider solid boundaries as purely repulsive walls with no bead flux. In the present paper we only consider two-dimensional flows and restrict, for simplicity, the dumbbells to lie in the flow plane. Although this assumption cannot be substantiated on physical grounds, we note that for a simple shear flow, at least, little difference can be observed between the predicted values for the stresses irrespective of whether polymer configuration space is assumed to be two-dimensional (a disc) or three-dimensional (a sphere) [9]. Our results may be extended without undue difficulty (although at greater computational cost) to higher dimensions.

Among other formulations for non-homogeneous flows of polymer solutions we may cite the body-tensor continuum formalism of Öttinger [25], the two-fluid Hamiltonian model of Mavrantzas and Beris [1,21] and the kinetic theory of Bhave et al. [4] that has been recently corrected and expanded upon by Curtiss and Bird [10]. The theory of Bhave et al. starts from the FP equation for Hookean dumbbells. Then, a number of approximations are used to obtain constitutive equations for the polymer number density and the stress tensor. In an illuminating paper dating from 1994, Beris and Mavrantzas [3] performed a detailed comparison of the three approaches mentioned above. Although the body-tensor continuum formalism of Öttinger [25] and the two-fluid Hamiltonian model of Mavrantzas and Beris [1,21] predicted the same equation for the polymer number density, the kinetic theory of Bhave et al. [4] led to the addition of an extra term in this equation. Beris and Mavrantzas identified the difficulty with the approach of Bhave et al. as being due to their retention only of the linear terms in a Taylor series expansion of the cdf in their expression for the polymer species concentration. The damaging consequences of this inconsistent approximation could be avoided by rederiving the mass flux equation using the force balance equation and by using a Taylor expansion for the cdf up to and including second-order terms. The resulting equation for the polymer number density was now the same as in the analyses of Öttinger and Mavrantzas and Beris. Neglect of second and higher-order terms in the

velocity gradient could be shown to lead to the same stress evolution equation under all three formulations. Note that no explicit equation for the polymer number density is required in this paper since we work throughout with the cdf ψ. The polymer number density may be calculated, however, at any time by integrating ψ over configuration space (see (16)).

The paper is organized as follows:

In Section 2 we recall the non-homogeneous FP equation for a dumbbell model and discuss the boundary conditions that will be prescribed for the cdf in the sequel. Explicit formulas for the different contributions to the Cauchy stress tensor are elucidated, where proper account is taken of the presence of physical boundaries. In Sections 2.1 - 2.3 weak forms of the FP equation are established, the stress calculator is explained and we discuss the discretization of the weak problem statement.

In Section 3 we illustrate the application of the theory of the previous section for the weakest unsteady non-homogeneous flow that exists: start-up non-homogeneous planar Poiseuille flow. Results are presented for a FENE fluid at different values of the ratio of molecular and macroscopic flow length scales. In generalization of an earlier result of Brunn and Grisafi [7] for Hookean dumbbells, we show that the equilibrium stress field is anisotropic, the first normal stress difference always being non-negative throughout the flow domain. In Section 3.2 the discretized equations in time and both physical and configuration space are developed in detail and the proposed numerical scheme then validated in the succeeding two subsections. In the first of these our theoretical predictions for the stress field in equilibrium are verified numerically. In the second, computations are shown to be in excellent quantitative agreement with a Brownian dynamics simulation. Comparable levels of accuracy between the two approaches (stochastic and deterministic) reveal a strong cost advantage in favour of the Fokker-Planck-based method proposed here. The main flow features are qualitatively the same as those seen by Brunn and Grisafi [7] and Petruccione and Biller [29] for the special cases of dumbbells having Hookean and weakly non-linear spring laws: polymer migration towards the channel centre, velocity and stress boundary layers in the vicinity of the channel walls and flattening of the velocity profile near the centreline.

We conclude the paper with some comments on the desirability of full chain simulations in a layer one polymer molecule distance from a solid boundary. These simulations are, however, deferred to a later paper.

2 A Fokker-Planck equation for non-homogeneous flows

In this paper we will consider the non-homogeneous flow of a dilute solution of FENE dumbbells in a Newtonian solvent. We denote the position vectors of the two beads in a dumbbell relative to some fixed origin by $\mathbf{r}_1$ and $\mathbf{r}_2$, and $\mathbf{R} = \mathbf{r}_2 - \mathbf{r}_1$ and $\mathbf{r}_c = \frac{1}{2}(\mathbf{r}_1 + \mathbf{r}_2)$ therefore denote, respectively, a dumbbell end-to-end vector and the position vector of the dumbbell's centre of mass.

Let $\mathbf{F}(\mathbf{R})$ denote the intermolecular spring force, $\mathbf{v}(\mathbf{r}_i)$ $(i = 1, 2)$ the solvent (possibly time-dependent) velocity at the position of the ith dumbbell bead and ζ a friction coefficient. Then the non-homogeneous FP equation for the cdf $\psi = \psi(\mathbf{r}_1, \mathbf{r}_2, t)$ may be written

$$\begin{aligned}\frac{\partial \psi}{\partial t} = &-\frac{\partial}{\partial \mathbf{r}_1} \cdot \left[\mathbf{v}(\mathbf{r}_1)\psi - \frac{1}{\zeta}\mathbf{F}(\mathbf{r}_1 - \mathbf{r}_2)\psi\right] \\ &-\frac{\partial}{\partial \mathbf{r}_2} \cdot \left[\mathbf{v}(\mathbf{r}_2)\psi - \frac{1}{\zeta}\mathbf{F}(\mathbf{r}_2 - \mathbf{r}_1)\psi\right] + \frac{kT}{\zeta}\frac{\partial^2 \psi}{\partial \mathbf{r}_1^2} + \frac{kT}{\zeta}\frac{\partial^2 \psi}{\partial \mathbf{r}_2^2}. \end{aligned} \tag{1}$$

In terms of the independent variables $\mathbf{r}_c$ and $\mathbf{R}$ the FP equation (1) may be rewritten as

$$\begin{aligned}\frac{\partial \psi^c}{\partial t} = &\frac{\partial}{\partial \mathbf{R}} \cdot \left(\frac{2kT}{\zeta}\frac{\partial \psi^c}{\partial \mathbf{R}} + \frac{2\mathbf{F}(\mathbf{R})\psi^c}{\zeta} + (\mathbf{v}(\mathbf{r}_c - \mathbf{R}/2) - \mathbf{v}(\mathbf{r}_c + \mathbf{R}/2))\psi^c\right) \\ &+\frac{\partial}{\partial \mathbf{r}_c} \cdot \left(\frac{kT}{2\zeta}\frac{\partial \psi^c}{\partial \mathbf{r}_c} - \frac{(\mathbf{v}(\mathbf{r}_c - \mathbf{R}/2) + \mathbf{v}(\mathbf{r}_c + \mathbf{R}/2))}{2}\psi^c\right), \end{aligned} \tag{2}$$

where we define $\psi^c(\mathbf{r}_c, \mathbf{R}, t) = \psi(\mathbf{r}_c - \mathbf{R}/2, \mathbf{r}_c + \mathbf{R}/2, t)$. We note in passing that the usual homogeneous flow assumption of constant $\nabla\mathbf{v}$ everywhere allows one to write $\mathbf{v}(\mathbf{r}_c - \mathbf{R}/2) - \mathbf{v}(\mathbf{r}_c + \mathbf{R}/2) = -\nabla\mathbf{v}(\mathbf{r}_c)\mathbf{R}$ and to assume the existence of a solution ψ independent of $\mathbf{r}_c$. Thus only the terms on the first line of the right-hand side of (2) appear in the homogeneous flow FP equation with a divergence-free velocity.

In order to assess the relative importance of different terms in (2) we introduce a characteristic macroscopic length scale L and a characteristic flow speed V. Then dimensionless variables $\mathbf{R}^*$, $\mathbf{r}_c^*$, $\mathbf{v}^*$, t^* may be introduced as follows:

$$\mathbf{R}^* = \mathbf{R}/l_0,\ \mathbf{r}_c^* = \mathbf{r}_c/L,\ \mathbf{v}^* = \mathbf{v}/V,\ t^* = t/(L/V), \tag{3}$$

where $l_0 = \sqrt{kT/H}$ is the expected magnitude of one component of the end-to-end vector of a Hookean dumbbell at equilibrium. We then define a non-dimensional maximum dumbbell extensibility $\sqrt{b}$ as $\sqrt{b} = R^*_{\max}$ and a characteristic relaxation time in the usual way as $\lambda = \zeta/4H$. Two dimensionless

groups that play an important role (especially expressed as a ratio) are the Deborah number De and the Péclet number Pe. These are defined in the present context as

$$De = \lambda V/L,\ Pe = 2\zeta LV/kT. \tag{4}$$

The Péclet number measures the importance of convective fluxes to diffusive fluxes in the polymeric molecules. With the dimensionless variables and groups introduced above, Eqn. (2) may be written as

$$\begin{aligned}\frac{D\psi^c}{Dt} =& \frac{\partial}{\partial \mathbf{R}} \cdot \left(\frac{1}{2De} \frac{\partial \psi^c}{\partial \mathbf{R}} + \frac{1}{2De} \mathbf{F}(\mathbf{R}) \psi^c + (\mathbf{v}(\mathbf{r}_c - \mathbf{R}/2) - \mathbf{v}(\mathbf{r}_c + \mathbf{R}/2)) \psi^c \right) \\ &+ \frac{1}{Pe} \frac{\partial^2 \psi^c}{\partial \mathbf{r}_c^2},\end{aligned} \tag{5}$$

where, for convenience, we have dropped the asterisks on the non-dimensionalized variables and $\frac{D}{Dt}$ denotes the material derivative

$$\frac{D}{Dt} = \frac{\partial}{\partial t} + \frac{(\mathbf{v}(\mathbf{r}_c - \mathbf{R}/2) + \mathbf{v}(\mathbf{r}_c + \mathbf{R}/2))}{2} \cdot \frac{\partial}{\partial \mathbf{r}_c}. \tag{6}$$

Under the non-dimensionalization described above the intermolecular spring force is written

$$\mathbf{F}(\mathbf{R}) = \frac{\mathbf{R}}{1 - \frac{R^2}{b}}. \tag{7}$$

We note from (5) that the diffusion term in real space has a coefficient $2De/Pe = l_0^2/(4L^2)$ times the magnitude of that of the diffusion term in configuration space. The ratio De/Pe has been interpreted by Bhave et al. [4] as representing the ratio of a diffusive length scale to a characteristic length scale of the macroscopic flow. This ratio is usually very small in real polymer systems ($\mathcal{O}(10^{-9})$ to $\mathcal{O}(10^{-7})$ when $L \approx 1$ cm [4]). The principal difference between stress and number density predictions based on the solution to (5) and those arising from the usual homogeneous flow FENE model are only to be seen in thin boundary layers. This is unsurprising since it is precisely near physical boundaries that a dumbbell is restricted in the configurations that it may adopt and the usual homogeneous flow assumption is most easily seen to be violated. The usual FENE model may thus be advocated for most polymer flows, where macroscopic length scales are much greater than the typical molecular length.

We recall that El-Kareh and Leal [11] expressed the hope that the retention of diffusion in real space could increase the stability of numerical methods, however small the diffusivity coefficient was. However, numerical experiments [31] reveal that for effective stabilization much larger diffusivity coefficients than those predicted by the kinetic theory are required.

We denote from now on the flow domain by Ω and assume that the boundary $\Gamma = \partial\Omega$ is an impenetrable wall. Following Biller and Petruccione [5,29], a no flux condition $\ll \dot{\mathbf{r}}_i \gg \cdot\, \mathbf{n} = 0$ on Γ with normal vector $\mathbf{n}$ is applied to the averaged bead velocity $\ll \dot{\mathbf{r}}_i \gg$ $(i = 1, 2)$. Assuming that $\mathbf{v}(\mathbf{r}_i) \cdot \mathbf{n} = 0$ on Γ, the velocity-space averaged force balance equations for the dumbbell beads lead to

$$\left(kT \frac{\partial \psi}{\partial \mathbf{r}_i} + \mathbf{F}(\mathbf{r}_i - \mathbf{r}_j)\psi \right) \cdot \mathbf{n} = 0 \text{ for } \mathbf{r}_i \in \Gamma, \tag{8}$$

and this may be re-expressed in the following form:

$$\left[\frac{\partial \psi^c}{\partial \mathbf{r}_c} \pm 2 \left(\frac{\partial \psi^c}{\partial \mathbf{R}} + \frac{1}{kT} \mathbf{F}(\mathbf{R}) \psi^c \right) \right] \cdot \mathbf{n} = 0, \text{ for } \mathbf{r}_c \pm \frac{\mathbf{R}}{2} \in \Gamma. \tag{9}$$

Multiplying (2) throughout by a test function $\varphi^c = \varphi^c(\mathbf{r}_c, \mathbf{R})$, integrating over all $(\mathbf{r}_c, \mathbf{R})$-space such that $\mathbf{r}_c \pm \mathbf{R}/2 \in \Omega$ and using integration by parts in configuration space, we have

$$\begin{aligned} \int_{\mathbf{r}_c} \int_{D(\mathbf{r}_c)} \frac{D\psi^c}{Dt} \varphi^c \, d\mathbf{R} d\mathbf{r}_c + \int_{\mathbf{r}_c} \int_{D(\mathbf{r}_c)} (\mathbf{v}(\mathbf{r}_c + \mathbf{R}/2) - \mathbf{v}(\mathbf{r}_c - \mathbf{R}/2)) \cdot \frac{\partial \psi^c}{\partial \mathbf{R}} \, \varphi^c d\mathbf{R} d\mathbf{r}_c \\ = \int_{\mathbf{r}_c} \int_{\Gamma^{\pm}(\mathbf{r}_c)} \left[\left(\frac{2kT}{\zeta} \frac{\partial \psi^c}{\partial \mathbf{R}} + \frac{2}{\zeta} \mathbf{F}(\mathbf{R}) \psi^c \right) \cdot \mathbf{n} \varphi^c \right] \, dS d\mathbf{r}_c \\ - \int_{\mathbf{r}_c} \int_{D(\mathbf{r}_c)} \left(\frac{2kT}{\zeta} \frac{\partial \psi^c}{\partial \mathbf{R}} + \frac{2}{\zeta} \mathbf{F}(\mathbf{R}) \psi^c \right) \cdot \frac{\partial \varphi^c}{\partial \mathbf{R}} \, d\mathbf{R} d\mathbf{r}_c \\ + \frac{kT}{2\zeta} \int_{\mathbf{r}_c} \int_{D(\mathbf{r}_c)} \frac{\partial^2 \psi^c}{\partial \mathbf{r}^2} \varphi^c \, d\mathbf{R} d\mathbf{r}_c, \end{aligned} \tag{10}$$

where $\Gamma^{\pm}(\mathbf{r}_c)$ are the parts of the boundary of

$$D(\mathbf{r}_c) = \{\mathbf{R} : |\mathbf{R}| < R_{\max}\} \bigcap \{\mathbf{R} : \mathbf{r}_c \pm \mathbf{R}/2 \in \Omega\},$$

on which $\mathbf{r}_c \pm \mathbf{R}/2 \in \Gamma$ and we have used the configuration boundary condition $\psi^c = \varphi^c = 0$ for $|\mathbf{R}| = R_{\max}$. Appealing to the boundary condition (9) we see that the weak form (10) may be further expressed as

$$\begin{aligned} \int_{\mathbf{r}_c} \int_{D(\mathbf{r}_c)} \frac{D\psi^c}{Dt} \varphi^c \, d\mathbf{R} d\mathbf{r}_c + \int_{\mathbf{r}_c} \int_{D(\mathbf{r}_c)} (\mathbf{v}(\mathbf{r}_c + \mathbf{R}/2) - \mathbf{v}(\mathbf{r}_c - \mathbf{R}/2)) \cdot \frac{\partial \psi^c}{\partial \mathbf{R}} \, \varphi^c d\mathbf{R} d\mathbf{r}_c \\ = \int_{\mathbf{r}_c} \int_{\Gamma^{\pm}(\mathbf{r}_c)} \left[\mp \frac{kT}{\zeta} \frac{\partial \psi^c}{\partial \mathbf{r}_c} \cdot \mathbf{n} \varphi^c \right] \, dS d\mathbf{r}_c \\ - \int_{\mathbf{r}_c} \int_{D(\mathbf{r}_c)} \left(\frac{2kT}{\zeta} \frac{\partial \psi^c}{\partial \mathbf{R}} + \frac{2}{\zeta} \mathbf{F}(\mathbf{R}) \psi^c \right) \cdot \frac{\partial \varphi^c}{\partial \mathbf{R}} \, d\mathbf{R} d\mathbf{r}_c \\ + \frac{kT}{2\zeta} \int_{\mathbf{r}_c} \int_{D(\mathbf{r}_c)} \frac{\partial^2 \psi^c}{\partial \mathbf{r}^2} \varphi^c \, d\mathbf{R} d\mathbf{r}_c. \end{aligned} \tag{11}$$

We shall return to consider the discretization of the weak form (11) in Section 2.3.

2.2 Stress tensor

Taking an arbitrary line in the (two-dimensional) dumbbell solution we consider the contribution to the elastic stress tensor at a point P with position vector $\mathbf{r}$ due to (a) the spring tension in dumbbells straddling the line at P and (b) changes in momentum brought about by beads passing through the line at P. Thus, denoting the total Cauchy stress tensor at P at time t by $\boldsymbol{\sigma}(\mathbf{r}, t)$ we decompose $\boldsymbol{\sigma}$ into the sum

$$\boldsymbol{\sigma} = \boldsymbol{\sigma}^S + \boldsymbol{\sigma}^C + \boldsymbol{\sigma}^K, \tag{12}$$

where $\boldsymbol{\sigma}^S$ denotes the solvent contribution, $\boldsymbol{\sigma}^C$ the spring tension contribution and $\boldsymbol{\sigma}^K$ the bead motion contribution. Expressions for these contributions in the case of non-homogeneous flows (see the book of Bird et al. [6]) are

$$\boldsymbol{\sigma}^S = -p\mathbf{I} + \eta_s \dot{\boldsymbol{\gamma}}, \tag{13}$$

$$\boldsymbol{\sigma}^C(\mathbf{r}, t) = \int_R \int_{s=0}^{1} \mathbf{R}\mathbf{F}(\mathbf{R}) \psi^c(\mathbf{r} + (s - 1/2)\mathbf{R}, \mathbf{R}, t)\, ds\, d\mathbf{R}, \tag{14}$$

and

$$\boldsymbol{\sigma}^K(\mathbf{r}, t) = -2n(\mathbf{r}, t) kT \mathbf{I}, \tag{15}$$

where

$$n(\mathbf{r}, t) = \int_R \psi^c(\mathbf{r} + \mathbf{R}/2, \mathbf{R}, t)\, d\mathbf{R}, \tag{16}$$

is the polymer number density. In writing the integrals appearing in (14) and

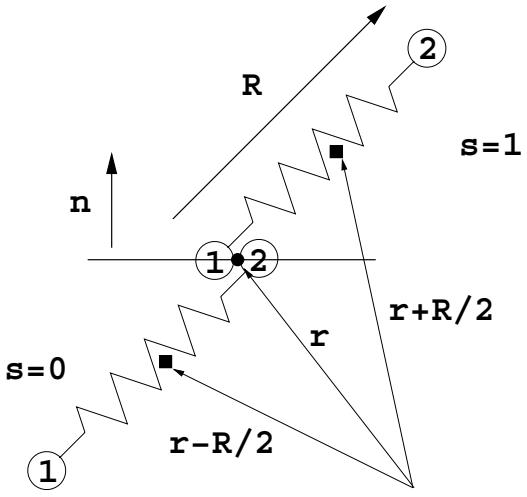

Fig. 1. Computation of $\boldsymbol{\sigma}^C$.

(16) we assume that ψ^c is set to zero for "forbidden" configurations i.e., those

that mean that a bead leaves the flow domain. The integration with respect to $\mathbf{R}$ can be thus performed over the whole of $\mathbb{R}^2$.

In (13) p is a pressure contribution from the solvent, η_s is the solvent viscosity and $\dot{\boldsymbol{\gamma}}$ is the rate-of-strain tensor $\nabla\mathbf{v} + \nabla\mathbf{v}^T$. (16) takes into account our assumption that the mass is concentrated at the beads of the dumbbells. (14) is slightly different from the equivalent formula of Bird et al. (see Eq.(13.3-5) of [6]) and takes account of the fact that ψ^c depends upon $\mathbf{r}_c$. As shown in Fig. 1, as the parameter s varies from 0 to 1 all dumbbells having end-to-end vector $\mathbf{R}$ and straddling the line at the point with position vector $\mathbf{r}$ are accounted for: from those with bead "2" having position vector $\mathbf{r}$ ($s = 0$) to those with bead "1" lying on the line ($s = 1$). If $\mathbf{n}$ is a unit normal vector to the line then $\mathbf{R} \cdot \mathbf{n}\psi^c(\mathbf{r} + (s - 1/2)\mathbf{R}, \mathbf{R}, t)ds$ is the expected number of dumbbells with end-to-end vector $\mathbf{R}$ whose centres of mass lie in a parallelogram of unit length, of height $\mathbf{R} \cdot \mathbf{n}ds$ and located at a distance $(s - 1/2)\mathbf{R} \cdot \mathbf{n}$ from the line.

As in [6] the bead motion contribution $\boldsymbol{\sigma}^K$ gives rise to an extra pressure term where equilibration in momentum space has been assumed in the derivation of (15). Note, unlike in [6], however, that the number density n is not, in general, constant.

2.3 Discretization in physical space and time and solution algorithm

Referring now to the second integral on the right-hand side of (11) and as discussed in previous work [9,19], preservation of the finiteness of the product $\mathbf{F}\psi^c$ on the parts of the configuration space boundary $R = \sqrt{b}$ that lie within the flow domain may be easily achieved by introducing a factorization of ψ of the form

$$\psi^c(\mathbf{r}_c, \mathbf{R}, t) = \psi_s(\mathbf{R})\alpha(\mathbf{r}_c, \mathbf{R}, t), \tag{17}$$

where $\psi_s(\mathbf{R}) = \left(1 - \frac{R^2}{R^2_{\max}}\right)^s$ for some $s \geq 1$, and rewriting the problem (11) in terms of the new variable α. This approach has been found [9,19] to be much more effective than simply setting ψ equal to zero on the boundary of configuration space.

For a two-dimensional problem (we can easily generalize to three dimensions) we will discretize the weak problem (11) by collocating in physical space and employing a Galerkin spectral method in configuration space. What is done in this paper is formally equivalent to introducing a test function

$$\varphi^c = \varphi^c_{kl} = \delta(\mathbf{r} - \mathbf{r}_{kl})\psi_s^{-1}(\mathbf{R})\sigma_{kl}(\mathbf{R}), \tag{18}$$

where δ is a delta function, $\mathbf{r}_{kl}$ is the position vector of the (k, l)th point in some collocation grid covering the interior physical flow domain and σ_{kl} an (as yet)

arbitrary function whose support is $D(\mathbf{r}_{kl})$. In each $D(\mathbf{r}_{kl})$, a suitably defined set Σ_{kl} of Lagrangian interpolants on a Gauss-Lobatto-Legendre (GLL) grid adapted to $D(\mathbf{r}_{kl})$ will be used for the test and trial functions in configuration space.

Allowing Δt to denote a time step and $\alpha_{kl}^n \in \Sigma_{kl}$ an approximation to $\alpha(\mathbf{r}_{kl}, \mathbf{R}, n\Delta t)$, where α has been introduced in (17), we may use an Euler method for (11) with an implicit treatment of the operators in configuration space and an explicit treatment for those in physical space:

$$
\begin{aligned}
&\int_{D(\mathbf{r}_{kl})} \left(\frac{\alpha_{kl}^{n+1} - \alpha_{kl}^n}{\Delta t} \right) \sigma_{kl} \, d\mathbf{R} \\
&+ \int_{D(\mathbf{r}_{kl})} \nabla \mathbf{v}(\mathbf{r}_{kl}) \mathbf{R} \cdot \frac{\partial}{\partial \mathbf{R}} \left(\psi_s \alpha_{kl}^{n+1} \right) \left(\psi_s^{-1} \sigma_{kl} \right) d\mathbf{R} \\
&+ \int_{D(\mathbf{r}_{kl})} \left(\frac{2kT}{\zeta} \frac{\partial}{\partial \mathbf{R}} \left(\psi_s \alpha_{kl}^{n+1} \right) + \frac{2}{\zeta} \mathbf{F}(\mathbf{R}) \psi_s \alpha_{kl}^{n+1} \right) \cdot \frac{\partial}{\partial \mathbf{R}} \left(\psi_s^{-1} \sigma_{kl} \right) \, d\mathbf{R} \\
&= \int_{\Gamma^{\pm}(\mathbf{r}_{kl})} \left[\left(\mp \frac{kT}{\zeta} \left(\frac{\partial \alpha}{\partial \mathbf{r}_c} \right)_{kl}^n \right) \cdot \mathbf{n} \sigma_{kl} \right] \, dS \\
&+ \int_{D(\mathbf{r}_{kl})} \left(\frac{kT}{2\zeta} \left(\frac{\partial^2 \alpha}{\partial \mathbf{r}_c^2} \right)_{kl}^n - \left(\frac{1}{2} (\mathbf{v}(\mathbf{r}_{kl} - \mathbf{R}/2) + \mathbf{v}(\mathbf{r}_{kl} + \mathbf{R}/2)) \cdot \frac{\partial \alpha}{\partial \mathbf{r}_c} \right)_{kl}^n \right) \sigma_{kl} \, d\mathbf{R}, \\
&+ \int_{D(\mathbf{r}_{kl})} (\nabla \mathbf{v}(\mathbf{r}_{kl}) \mathbf{R} - \mathbf{v}(\mathbf{r}_{kl} + \mathbf{R}/2) + \mathbf{v}(\mathbf{r}_{kl} - \mathbf{R}/2)) \cdot \frac{\partial}{\partial \mathbf{R}} \left(\psi_s \alpha_{kl}^n \right) \left(\psi_s^{-1} \sigma_{kl} \right) d\mathbf{R} \\
&\qquad\qquad\qquad\qquad\qquad\qquad\qquad\qquad\qquad\qquad \forall \sigma_{kl} \in \Sigma_{kl},
\end{aligned}
\tag{19}
$$

where $(\cdot)_{kl}^n$ denotes a suitable approximation to the quantity in parentheses at $t = n\Delta t$ and $\mathbf{r} = \mathbf{r}_{kl}$. Note that the velocity difference $\mathbf{v}(\mathbf{r}_{kl} + \mathbf{R}/2) - \mathbf{v}(\mathbf{r}_{kl} - \mathbf{R}/2)$ is approximated in the implicit treatment of operators in configuration space by $\nabla \mathbf{v}(\mathbf{r}_{kl})\mathbf{R}$. This allows us to use the fast solver for the FP equation introduced in [19]. The error entailed by this approximation is compensated by the term with $(\nabla \mathbf{v}(\mathbf{r}_{kl})\mathbf{R} - \mathbf{v}(\mathbf{r}_{kl} + \mathbf{R}/2) + \mathbf{v}(\mathbf{r}_{kl} - \mathbf{R}/2))$ in the explicit part of (19). The last term is usually very small hence it should not affect heavily the overall stability of the scheme. A Gauss-Lobatto quadrature formula is to be used in this paper for the evaluation of the integrals over $D(\mathbf{r}_{kl})$. The computation of the partial derivatives of α in physical space appearing on the right-hand side of (19) is normally performed by taking a weighted sum of physical nodal values of α. Therefore a double sum - for the quadrature rule and the difference formulae required for the physical derivatives - is needed and care must be taken to ensure that each term in the double sum makes sense i.e. no attempt is made to evaluate a nodal value α_{pq}^n (say) of α at a quadrature point in configuration space which is outside $D(\mathbf{r}_{pq})$. No such difficulty is encountered for discretizations where the cdf is assumed to be independent of $\mathbf{r}_c$ (homogeneous flow) since of course in this case configuration space is, by assumption, the same for all physical points.

Details of the above discretizations and solution algorithm in the case of a simple test problem are provided in the next section.

3 Example: Start-up non-homogeneous planar Poiseuille flow.

We now wish to apply the method described in the foregoing section to non-homogeneous start-up planar Poiseuille flow of a FENE fluid. The flow geometry is shown in Fig. 2(a) and consists of two plates $y = \pm d$ between which a dilute polymer solution flows under a constant pressure gradient. We will compute a solution of the form $\psi^c = \psi^c(y, \mathbf{R}, t)$, $\mathbf{v} = (v_x(y,t), 0)$, $p = -Px + \tilde{p}(y,t)$ where P is the negative imposed streamwise pressure gradient. The equation of conservation of momentum can be written then as

$$\rho \frac{\partial v_x}{\partial t} = P + \eta_s \frac{\partial^2 v_x}{\partial y^2} + \frac{\partial \sigma^C_{xy}}{\partial y}, \tag{20}$$

$$\frac{\partial \tilde{p}}{\partial y} = \frac{\partial \sigma^C_{yy}}{\partial y} + \frac{\partial \sigma^K_{yy}}{\partial y}, \tag{21}$$

where ρ is the fluid density. The last equation can be integrated to give the full form of the pressure $p = -Px + \sigma^C_{yy} + \sigma^K_{yy} + const.$

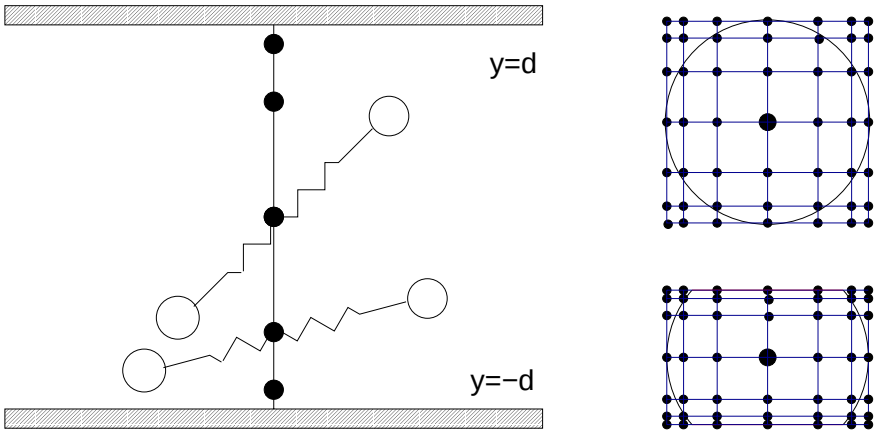

Fig. 2. (a) Flow between two parallel walls and Gauss collocation grid, (b) configuration spaces $D(y)$ for two different values y_k of y with superposed Gauss-Lobatto grids

Previous simulations with non-homogeneous flow models have included the use of a two-fluid Hamiltonian [21] in investigations of instabilities in cone-and-plate and parallel plate rheometers [23] and of stress gradient-induced migration effects in the viscoelastic Taylor-Couette problem [1]. Rectilinear shear flows of Hookean dumbbells have been studied by, amongst others, Bhave et

al. [4] using a finite difference method. Biller and Petruccione [5] used a Brownian dynamics simulation for simple shear flow of dumbbells having both a Hookean spring force law and a simple nonlinear modification to this force law, obtained from the FENE spring force law for small values of dumbbell extension R. The same technique was used by the authors to investigate non-homogeneous pressure-driven flows of the same dumbbell solutions [29]. The present work applies a new method (see Sections 2.1 and 2.3) to the planar Poiseuille flow of dumbbells having a FENE force law without the same restriction on the magnitude of the extension R. The results therefore generalize what has gone before. In addition, our equilibrium results in Section 3.1 for the FENE fluid generalize earlier results by Brunn and Grisafi [7] for Hookean dumbbells. In particular, we show analytically that the stress field at equilibrium is anisotropic with the first normal stress difference always non-negative.

3.1 Equilibrium: kinetic theory

In this subsection we summarize some new results from the kinetic theory of a FENE dumbbell solution under equilibrium conditions in the channel shown in Fig. 2(a). The results presented here generalize those of Brunn and Grisafi [7] who considered Hookean dumbbells in equilibrium.

Writing the spring force contribution to the equilibrium stress tensor as $\boldsymbol{\sigma}_{eq}^{C}$ it may be shown (see Appendix A) that

$$\sigma_{eq,xx}^{C} - \sigma_{eq,yy}^{C} = kT \int_{\{|\mathbf{R}|<R_{\max}\}\bigcap\{|R_y|\geq d-|y|\}} \left(\frac{d-|y|}{|R_y|}\right) \psi_0(\mathbf{R})\, d\mathbf{R} \geq 0, \quad (22)$$

where

$$\psi_0(\mathbf{R}) = C\left(1 - \frac{|\mathbf{R}|^2}{R_{\max}^2}\right)^{b/2}, \quad (23)$$

is the equilibrium cdf for the homogeneous-flow FENE model and C is a normalizing constant. The inequality in Eqn. (22) is strict provided $|y| \in (d - R_{\max}, d)$. Hence the equilibrium stress field is anisotropic, as observed by Brunn and Grisafi [7] for Hookean dumbbells.

Troubling as an anisotropic stress field at equilibrium may appear at first sight, there is in fact no inconsistency between this and equilibrium conditions since

$$\nabla \cdot \left(\boldsymbol{\sigma}_{eq}^{C} + \boldsymbol{\sigma}_{eq}^{K}\right) = \mathbf{0}. \quad (24)$$

This result is derived in Appendix A.

3.2 Discretization and solution algorithm

3.2.1 Approximation of derivatives in physical space

For the simple case of a one-dimensional flow in a channel illustrated in Fig. 2(a) a discretization may be done relatively easily and efficiently. Since the most interesting phenomena are near the boundaries $y = \pm d$, we choose the collocation points to be the Gauss-Legendre (GL) points y_k $(k = 1, \cdots, N_{GL})$ (for some choice of the parameter N_{GL}) mapped onto the interval $(-d, d)$. Note that this set of collocation points does not include the end points $\pm d$ since the cdf $\psi^c(y, \mathbf{R}, t)$ has no meaning for y lying on the boundary (configuration space has zero two-dimensional measure there). Fig. 2(b) illustrates the configuration spaces $D(y)$ for two different choices of y.

We now seek approximations α_k^n of $\alpha(y_k, \mathbf{R}, t)$ at discrete times $t_n = n\Delta t$ and discrete physical points y_k and satisfying the scheme (19), rewritten in this case as

$$\begin{aligned}
&\left(\frac{\alpha_k^{n+1} - \alpha_k^n}{\Delta t}, \sigma_k\right)_{D(y_k)} + A_k(\alpha_k^{n+1}, \sigma_k) \\
&= -\frac{kT}{\zeta}\left(n_y \left(\frac{\partial \alpha}{\partial y}\right)_k^n, \sigma_k\right)_{\Gamma(y_k)} + \frac{kT}{2\zeta}\left(\left(\frac{\partial^2 \alpha}{\partial y^2}\right)_k^n, \sigma_k\right)_{D(y_k)} \\
&+ \left(\left(v_x(y_k - R_y/2) - v_x(y_k + R_y/2) + \frac{\partial v_x(y_k)}{\partial y} R_y\right) \frac{\partial}{\partial R_x}\left(\psi_s \alpha_k^n\right), \psi_s^{-1}\sigma_k\right)_{D(y_k)}, \\
&\qquad\qquad \forall \sigma_k \in \Sigma_k,
\end{aligned} \tag{25}$$

where Σ_k denotes the discretization space in configuration space, $(\cdot, \cdot)_{D(y_k)}$ the L^2 inner product over $D(y_k)$, $n_y = \mathrm{sgn(y)}$ and

$$\begin{aligned}
A_k(\alpha, \sigma) = &\left(\frac{2kT}{\zeta}\frac{\partial}{\partial \mathbf{R}}\left(\psi_s \alpha\right) + \frac{2}{\zeta}\mathbf{F}(\mathbf{R})\psi_s \alpha, \frac{\partial}{\partial \mathbf{R}}\left(\psi_s^{-1}\sigma\right)\right)_{D(y_k)} \\
&+ \frac{\partial v_x}{\partial y}(y_k)\left(R_y \frac{\partial}{\partial R_x}\left(\psi_s \alpha\right), \psi_s^{-1}\sigma\right)_{D(y_k)}.
\end{aligned} \tag{26}$$

Using a first-order approximation for the derivative $\frac{\partial \psi}{\partial y}$ in the boundary inte-

gral, we obtain

$$\left(\frac{\alpha_k^{n+1}-\alpha_k^n}{\Delta t},\sigma_k\right)_{D(y_k)} + A_k(\alpha_k^{n+1},\sigma_k)$$
$$= \frac{kT}{\zeta}\left(\frac{\alpha_{k+j}^n-\alpha_k^n}{h_k^+},\sigma_k\right)_{\Gamma(y_k)} + \frac{kT}{2\zeta}\left(\left(\frac{\partial^2\alpha}{\partial y^2}\right)_k^n,\sigma_k\right)_{D(y_k)}$$
$$+\left(\left(v_x(y_k-R_y/2)-v_x(y_k+R_y/2)+\frac{\partial v_x(y_k)}{\partial y}R_y\right)\frac{\partial}{\partial R_x}\left(\psi_s\alpha_k^n\right),\psi_s^{-1}\sigma_k\right)_{D(y_k)},$$
$$\forall\sigma_k\in\Sigma_k, \tag{27}$$

where j is $-n_{y_k}$ so that $y_{k+j}\in(-|y_k|,|y_k|)$ and $h_k^+ = |y_{k+j}-y_k|$. In what follows below h_k^- will denote the step size $|y_{k-j}-y_k|$.

Equation (27) is the scheme we shall use for our simulations. $\left(\frac{\partial^2\alpha}{\partial y^2}\right)_k^n$ still needs to be specified. This discrete operator in physical space depends upon the point of configuration space where it is applied. Indeed, if y_{k-j} is defined and $\mathbf{R}\in D(y_{k-j})$, then we can use the standard central difference approximation:

$$\left(\frac{\partial^2\alpha}{\partial y^2}\right)_k^n(\mathbf{R}) = \frac{2}{h_k^+ + h_k^-}\left(\frac{\alpha_{k+j}^n(\mathbf{R})-\alpha_k^n(\mathbf{R})}{h_k^+}+\frac{\alpha_{k-j}^n(\mathbf{R})-\alpha_k^n(\mathbf{R})}{h_k^-}\right).$$

Otherwise, $\alpha_{k-j}^n(\mathbf{R})$ is not defined and we construct instead a first-order approximation for $\frac{\partial^2\alpha}{\partial y^2}(y_k,\mathbf{R},t_n)$ using the boundary condition (8).

Remark: Although only first-order discretizations in physical space as described above have been used for the numerical results to be presented in Sections 3.3.2 and 3.3.3 this is for the sake of illustration and simplicity only. Extension to second- and higher-order approximations to the first and second derivatives of α with respect to y are entirely straightforward.

3.2.2 Discretization in configuration space

For each y_k the corresponding configuration space is the intersection of the disc $R<\sqrt{b}$ and the rectangle $(R_x,R_y)\in(-\sqrt{b},\sqrt{b})\times(-d_k,d_k)$ where $d_k = 2(d-|y_k|)$. We introduce in this rectangle the GLL points $(R_x^{k,i},R_y^{k,j})$, $i=1,\ldots,N_x^k$, $j=1,\ldots,N_y^k$, and then expand α in terms of a tensorized basis consisting of Lagrange interpolating polynomials based upon these points. That is, we write

$$\alpha_k^n(\mathbf{R}) = \sum_{i=1}^{N_x^k}\sum_{j=1}^{N_y^k}\widehat{\alpha}_{ijk}^n H_i^k(R_x)H_j^k(R_y), \tag{28}$$

where the coefficients $\widehat{\alpha}_{ijk}^n$ are set to zero for polynomials corresponding to grid points outside the disc, i.e. such that $(R_x^{k,i})^2+(R_y^{k,j})^2\geq b$. In other words, the

discrete space Σ_k to which both trial and test functions in configuration space belong, is defined to consist of polynomials $H_i^k(R_x)H_j^k(R_y)$ with i,j such that $(R_x^{k,i})^2 + (R_y^{k,j})^2 < b$. For the results presented in Section 3.3 we have chosen for simplicity the number of points N_x^k and N_y^k in the two directions equal to some constant N_{GLL} (say), independent of k.

We recall that the parameter s was set equal to 2 in [9,19] and that α was only required to be bounded on $R = \sqrt{b}$ in these papers. However, in the present approach α approximated by (28) is already approximately zero at $R = \sqrt{b}$ so that the parameter s may be set equal to unity here.

The configuration step for a given $y = y_k$ may be performed efficiently and the reader is referred to [19] for an explanation of the main ideas involved.

3.2.3 Computation of the polymer density n and elastic stress $\boldsymbol{\sigma}^C$

Direct computation of $\boldsymbol{\sigma}^C$ by a discrete variant of (14) would involve the interpolations of α between different configuration spaces $D(y_k)$. We found in practice that better accuracy and stability could be achieved by an alternative way of computation of $\boldsymbol{\sigma}^C$ that does not involve such interpolations.

Instead of (14) we use its weak form:

$$\begin{aligned}
&\int_{-d}^{d} \boldsymbol{\sigma}^C(y,t)H(y)dy \\
&\quad = \int_{-d}^{d}\int_R \int_{s=0}^{1} \mathbf{RF}(\mathbf{R})\psi^c(y+(s-1/2)R_y,\mathbf{R},t)H(y)\; dsd\mathbf{R}dy \\
&\quad = \int_{-d}^{d}\int_R \mathbf{RF}(\mathbf{R})\psi^c(y,\mathbf{R},t)\; \left(\int_{s=0}^{1} H(y-(s-1/2)R_y)ds\right) d\mathbf{R}dy, \quad (29)
\end{aligned}$$

the test function $H(y)$ here being set to 0 outside the interval $(-d,d)$. We now set $H(y)$ equal to the i-th interpolating Lagrangian polynomial $h_i(y)$ based on the physical collocation points $\{y_j\}$ $(h_i(y_j) = \delta_{ij})$ and evaluate the integral in $(-d,d)$ by using the Gauss-Legendre quadrature rule with weights $\{\omega_k\}_{k=1}^{N_{GL}}$. We thus obtain an approximation for $\boldsymbol{\sigma}^C$ at the grid points

$$\boldsymbol{\sigma}^C(y_i,t_n) = \sum_{k=1}^{N_{GL}} \frac{\omega_k}{\omega_i} \int_{D(y_k)} \mathbf{RF}(\mathbf{R})\psi_s(\mathbf{R})\alpha_k^n \int_{s=0}^{1} H(y_k-(s-1/2)R_y)\; dsd\mathbf{R}. \quad (30)$$

The same idea can be applied to the computation of the number density:

$$n(y_i,t_n) = \sum_{k=1}^{N_{GL}} \frac{\omega_k}{\omega_i} \int_{D(y_k)} \psi_s(\mathbf{R})\alpha_k^n H(y_k - R_y/2)\; d\mathbf{R}. \quad (31)$$

3.3 Numerical results

The numerical results in this section will be presented in terms of the dimensionless ordinate y/d. A dimensionless streamwise velocity and polymer number density may be defined as $v_x/(d/\lambda)$ and n/n_{avg}, respectively, where n_{avg} is the average polymer number density. Accordingly, the natural unit for stresses and pressure is $n_{avg}kT$, and for the viscosity $n_{avg}kT\lambda$. We choose the following parameter set: $\sqrt{b} = 3$, $\eta_s = 0.2 n_{avg}kT\lambda$. The dimensionless pressure gradient $P^* = P/(n_{avg}kT)$ is set equal to 2 or 10. The number N_{GL} of GL collocation points in real space and the number N_{GLL} of GLL points in each direction in configuration space vary between 16 and 30. The time step Δt is set equal to 0.01λ for $P^* = 2$ and to 0.0025λ for $P^* = 10$. We consider only zero Reynolds number flow.

After integration with respect to y, the inertialess momentum equation (20) becomes

$$\eta_s \frac{\partial v_x}{\partial y} = -Py - \sigma_{xy}^C + K, \tag{32}$$

where, in general, K is an unknown constant (although equal to zero for symmetric velocity profiles v_x). We approximate the velocity v_x by using a basis consisting of interpolating polynomials based on a GLL grid of $N_{GL} + 1$ points. The discrete system for determining the approximation of the velocity may then be obtained by collocating (32) at the points $\{y_k\}$, $k = 1, \ldots, N_{GL}$, and setting v_x to zero at $y = \pm d$. We thus have $N_{GL} + 2$ equations for the components of v_x and K.

In the presentation of the results we shall make frequent reference to the parameter ratio

$$\frac{l_0}{d} = \frac{1}{d}\sqrt{\frac{kT}{H}}, \tag{33}$$

which measures a characteristic equilibrium length scale for the dumbbell relative to the wall separation distance. Thus, the smaller the value of l_0/d the smaller the influence of the walls on the flow between them, except for an increasingly thin boundary layer. Indeed, for $l_0/d = 0$ the usual FENE solution for plane Poiseuille flow is recaptured. An alternative way of viewing l_0/d is in its equivalent form $\sqrt{8De/Pe}$ where the Deborah number De and Péclet number Pe have been introduced already in Section 2.

3.3.1 Equilibrium

In Fig. 3 we provide numerical confirmation in the case $l_0/d = 0.1$ that at equilibrium σ_{xx}^C is indeed greater than or equal to σ_{yy}^C throughout the gap between the plates $y = \pm d$. In Fig. 4 we plot σ_{yy}^C at equilibrium for values of

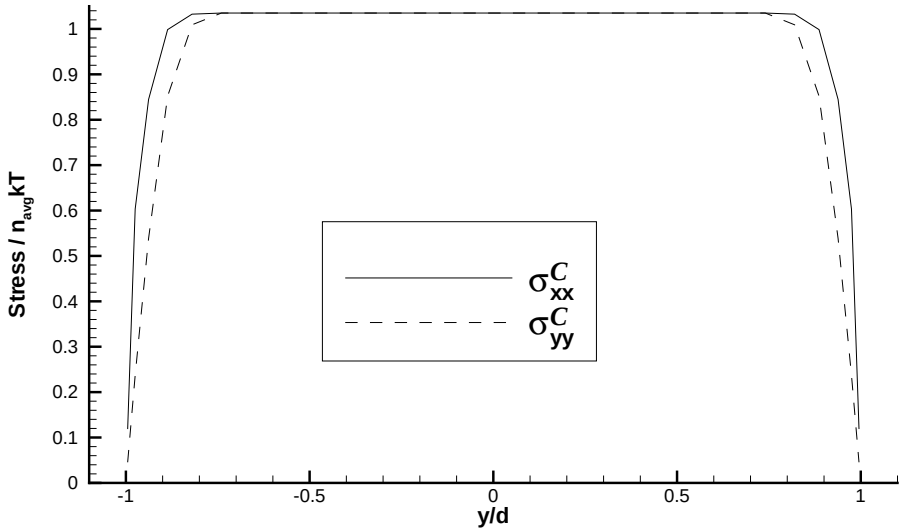

Fig. 3. Normal components of $\boldsymbol{\sigma}^C$ at equilibrium; $l_0/d = 0.1$, $N_{GL} = 24$, $N_{GLL} = 20$.

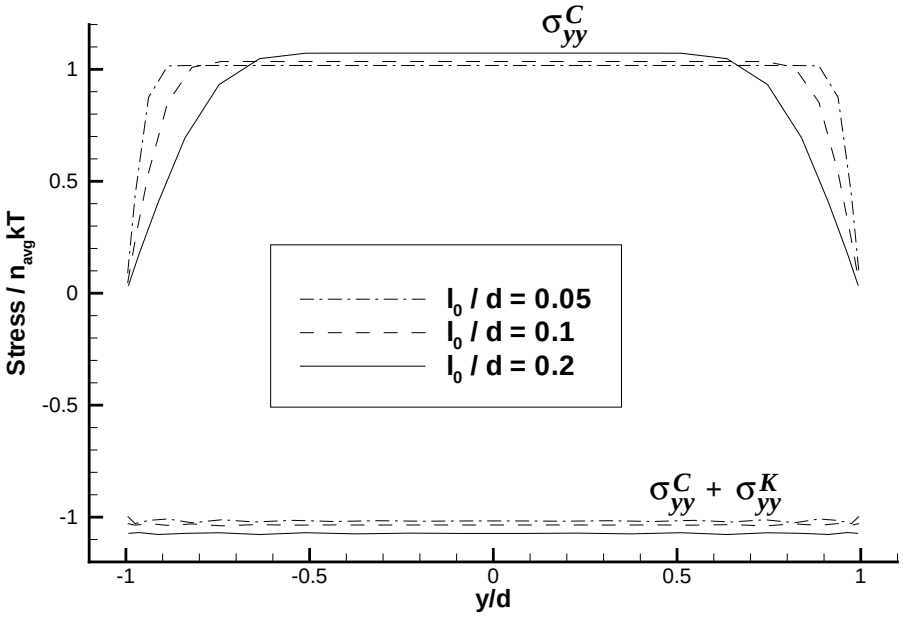

Fig. 4. σ^C_{yy} and $\sigma^C_{yy} + \sigma^K_{yy}$ at equilibrium; $N_{GL} = 24$, $N_{GLL} = 20$.

$l_0/d = 0.05$, 0.2 and 1. Although σ^C_{yy} varies strongly with y in the boundary layers the lower plot shows that $\sigma^C_{yy} + \sigma^K_{yy}$ is a constant, in confirmation of (A.17).

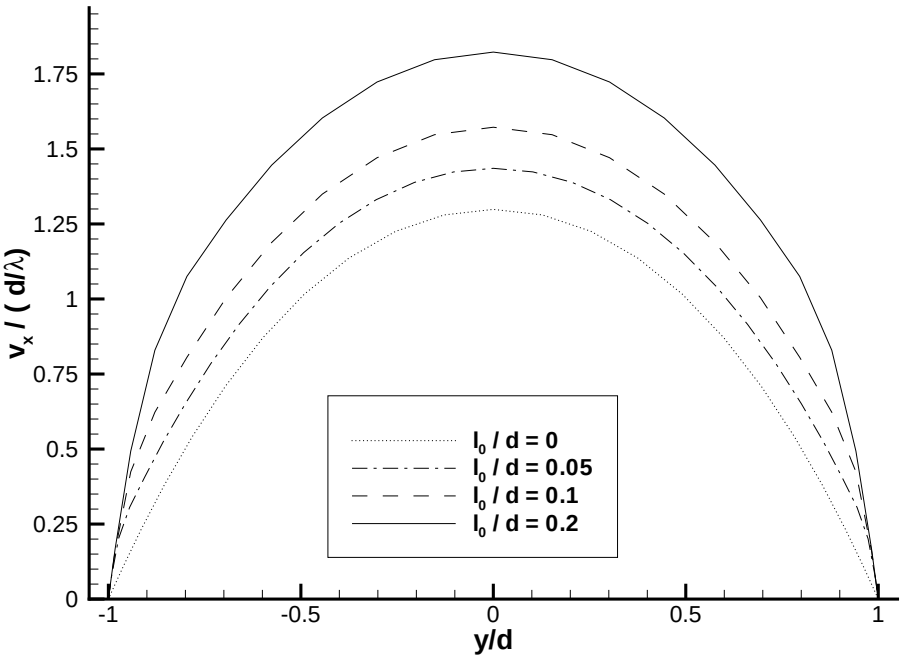

Fig. 5. Velocity v_x for different ratios l_0/d; $N_{GL} = N_{GLL} = 24$.

3.3.2 Planar start-up non-homogeneous Poiseuille flow: effect of varying l_0/d

In Figs. 5-6 the profiles of the steady-state dimensionless velocity v_x and of the polymer number density n, calculated with an applied negative dimensionless pressure gradient $P^* = 2$ are shown for different values of l_0/d. For $l_0/d = 0$ (equivalent to the homogeneous flow FENE model) the polymer number density is a constant. However, we observe that as l_0/d increases from 0 to 1 the wall effects become stronger and polymer migrates from the channel walls $y = \pm d$ towards the centre of the channel. As a consequence the velocity gradient steepens near the walls in order to maintain the total shear stress and the profile flattens near the channel centre since the total viscosity increases there. These effects are also evident as we increase the applied pressure gradient P^* from 2 to 10 whilst fixing $l_0/d = 0.1$. As well as the obvious increase in mass flow rate (see Fig. 7) we see that by dividing each of the profile values by their maximum value (see Fig. 8) the rescaled profiles are typical of those at lower and higher shear rates in a shear-thinning fluid, the profile flattening near the centreline for the higher pressure gradient. From Eqn. (14) it should be clear that the spring tension contribution $\boldsymbol{\sigma}^C$ to the total Cauchy stress vanishes at the boundaries $y = \pm d$ since configurational space shrinks to a line (and therefore to a region in two-dimensional space of measure zero!) From a micro-mechanical point of view $\boldsymbol{\sigma}^C$ must be zero at a solid wall since no dumbbells can straddle this boundary. Thus, for $l_0/d > 0$ boundary layers are to be seen

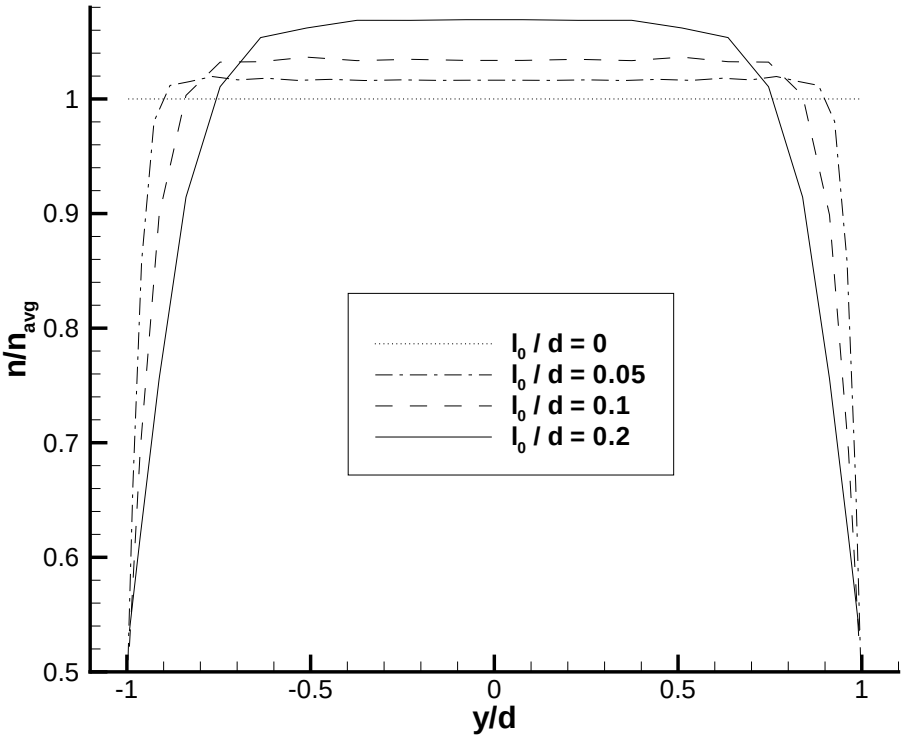

Fig. 6. Polymer number density n for different ratios l_0/d; $N_{GL} = N_{GLL} = 24$.

in Figs. 9-11. As l_0/d increases from 0 to 1 the number density of polymers in the bulk flow also increases and leads to an increase in the magnitude of the stress there relative to the homogeneous flow (constant n) case.

3.3.3 Planar start-up non-homogeneous Poiseuille flow: comparison between deterministic and stochastic simulations

In Figs. 12 and 13 we show the results of testing the convergence of our method with mesh refinement and compare our results with those obtained with stochastic simulations as explained in [5,29]. For the stochastic simulations we implemented an Euler method with an implicit treatment of the spring force term using M pseudo-random realizations and an equispaced grid in $(-d, d)$ with N_P points. All the simulations were performed over the time interval $(0, 6\lambda)$ with the time step $\Delta t = 0.01\lambda$. All the results of stochastic simulations were averaged over $(4\lambda, 6\lambda)$.

As can be seen from Figs. 12-13, excellent convergence is achieved for the deterministic method with the grid $N_{GL} = N_{GLL} = 20$ and the stochastic method with $M = 2 \times 10^6$ and $N_P = 50$ for $l_0/d = 0.1$, there being no obvi-

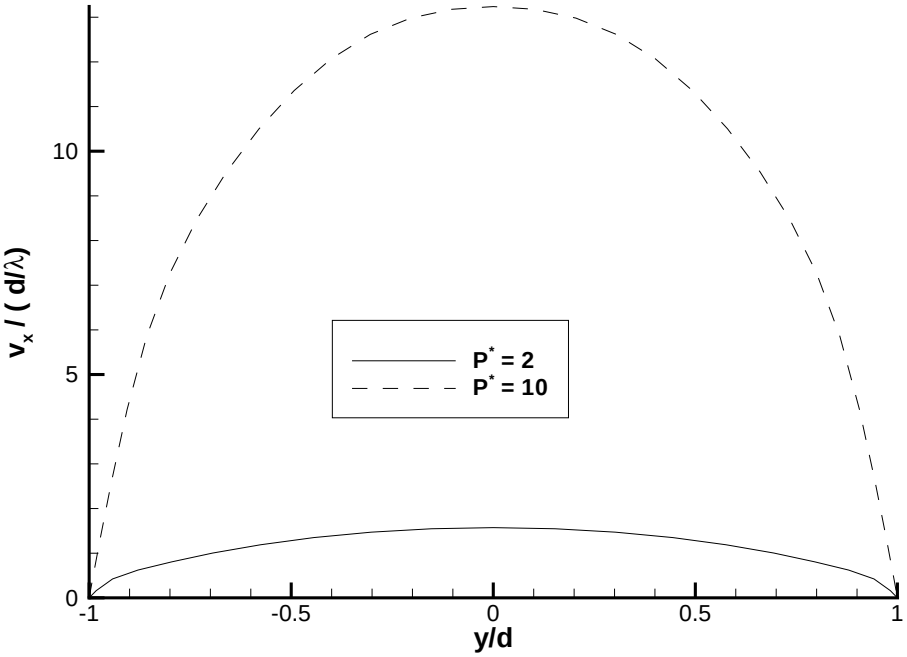

Fig. 7. Velocity for $P^* = 2$ and $P^* = 10$; $N_{GL} = N_{GLL} = 30$.

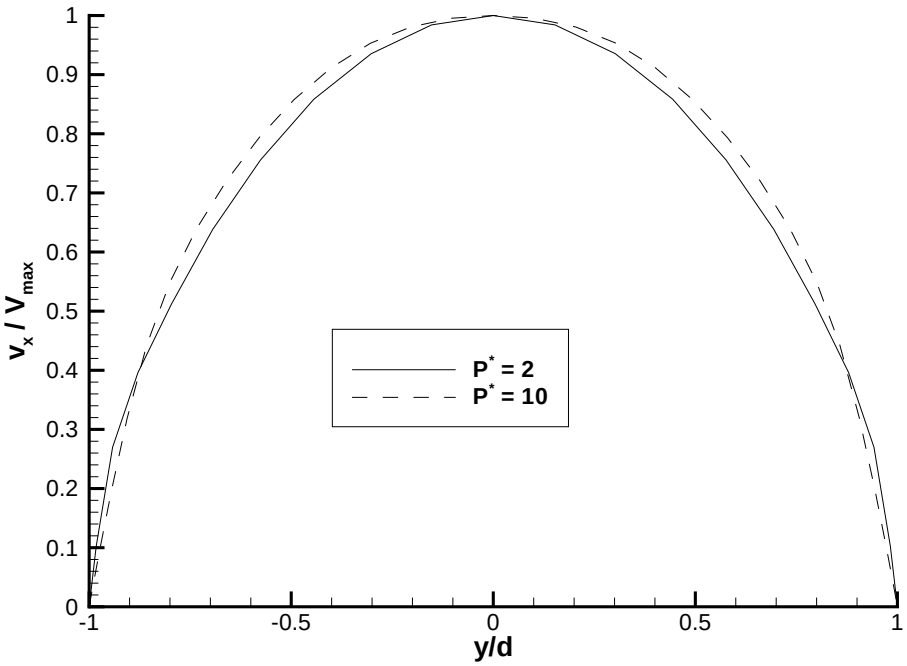

Fig. 8. Normalized velocity for $P^* = 2$ and $P^* = 10$; $N_{GL} = N_{GLL} = 30$.

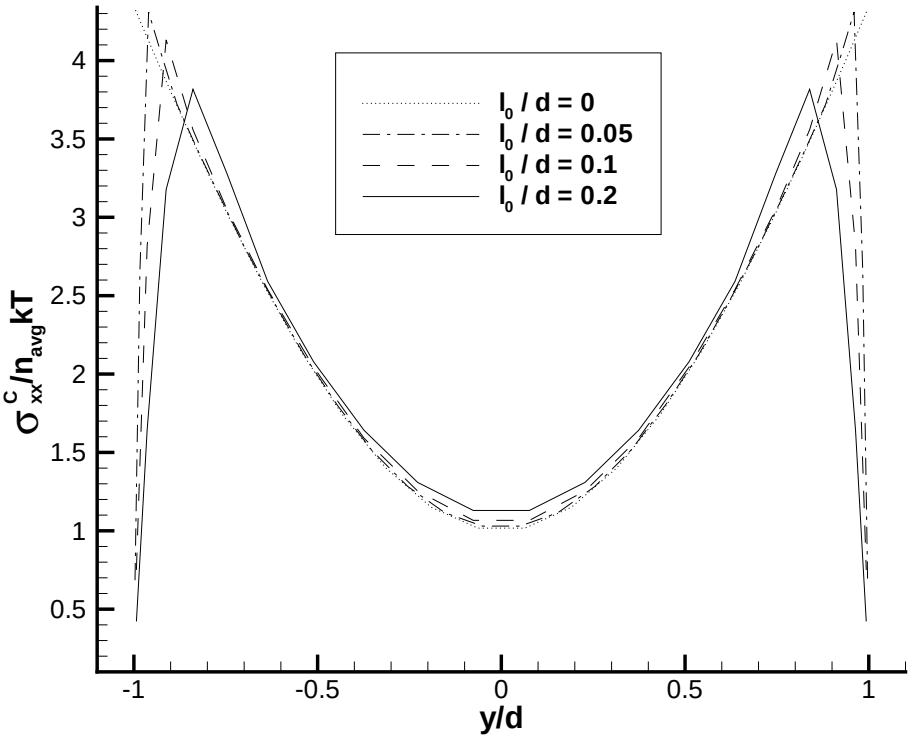

Fig. 9. Stress component σ_{xx}^C for different ratios l_0/d; $N_{GL} = N_{GLL} = 24$.

ous difference between the profiles of v_x and n computed with either method. Fig. 13 confirms the presence of significant noise in the results for the polymer number density for the stochastic simulations with the smaller number of pseudo-random realizations $M = 2 \times 10^4$. The same observation of noise has been made for the stochastic computations of the stress tensor components, although these results are not shown here. However, the stochastic method with $M = 2 \times 10^4$ requires CPU times larger than those needed for the deterministic simulations with $N_{GL} = N_{GLL} = 16$, which already demonstrate good accuracy. If we compare the converged (in the eyeball norm) solutions, the enormous cost advantage of the deterministic method over the stochastic method is evident.

3.3.4 Planar start-up non-homogeneous Poiseuille flow: effect of varying b

In order to assess the impact on the flow field of varying the dimensionless maximum dumbbell extensibility we have fixed $P^* = 2$, $l_0/d = 0.2$ and chosen $b = 9$ and 1×10^6. Numerical experiments for the present problem have indicated that for values of $b \gtrsim 1 \times 10^6$ no visible change in the flow field occurs and the intermolecular spring may then be considered to be Hookean (and the

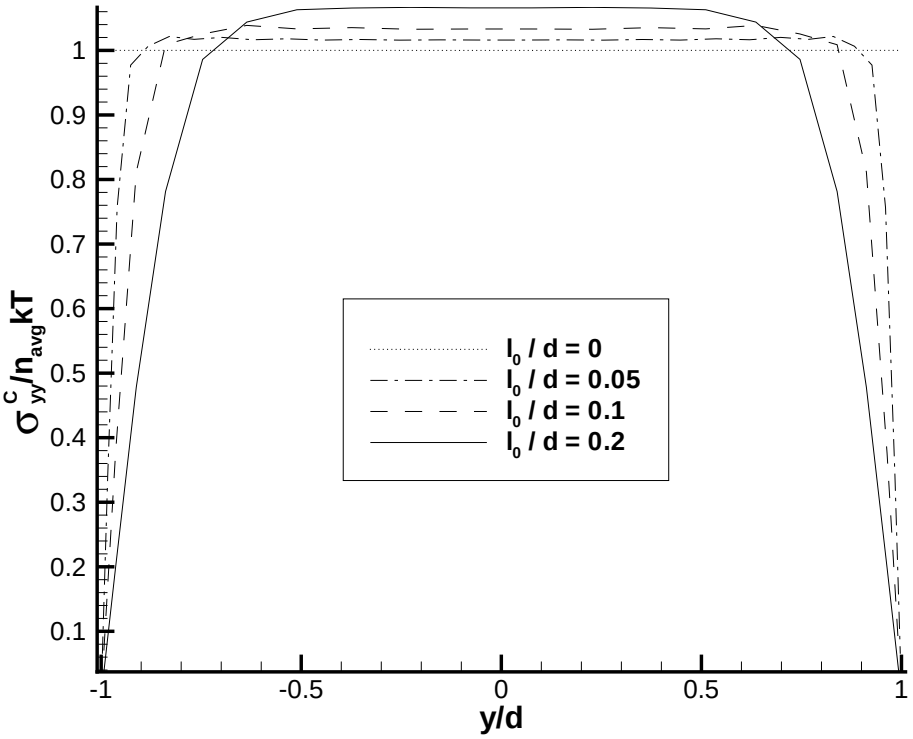

Fig. 10. Stress component σ^C_{yy} for different ratios l_0/d; $N_{GL} = N_{GLL} = 24$.

model thus that of an Oldroyd B fluid). The results were obtained using our stochastic simulation method with $M = 1 \times 10^5$ pseudo-random realizations on an equispaced grid in $(-d, d)$ having $N_P = 101$ points and a time step $\Delta t = 0.0025\lambda$. The data represented in Figs. 14 and 15 was generated by running the simulations over a time interval $[0, 50\lambda]$ and averaging the velocity and stress values over $t \in [45\lambda, 50\lambda]$.

In Fig. 14 it may be seen that under the same pressure gradient the mass flow rate of the FENE fluid is higher than for the Oldroyd B fluid, due to shear-thinning effects. The unbounded extensibility of the Hookean intermolecular springs of the Oldroyd B model results in elastic stresses that are higher than for the finitely extensible model and this is evidenced in Fig. 15

4 Conclusions

In this paper we have introduced a new implementation of a high-order numerical method based on the Fokker-Planck equation for non-homogeneous flows of dilute polymer solutions. Results have been presented for the FENE model,

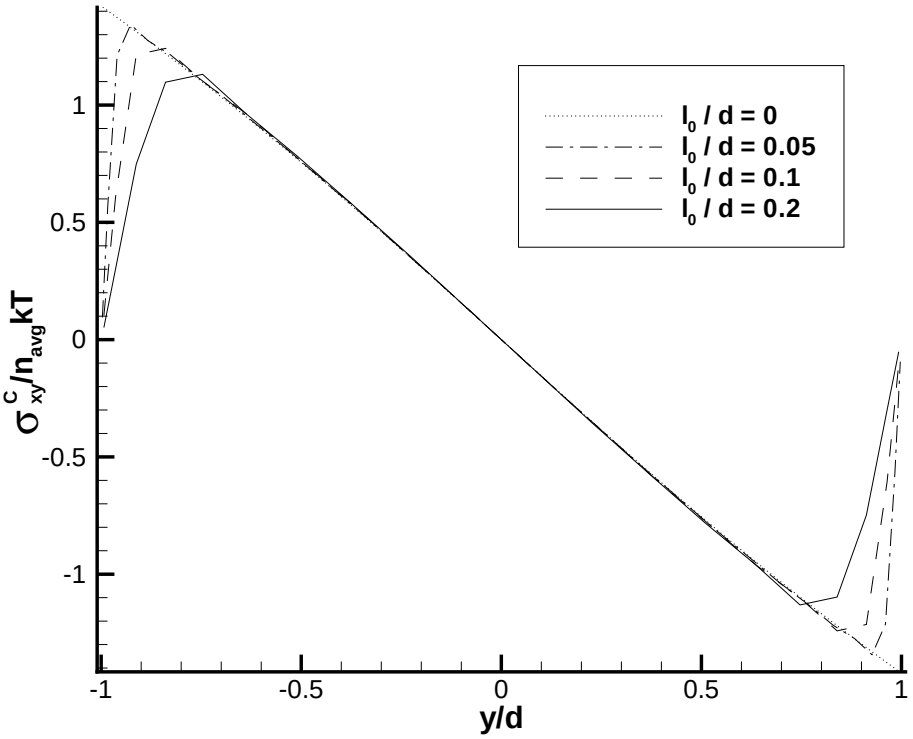

Fig. 11. Stress component σ_{xy}^{C} for different ratios l_0/d; $N_{GL} = N_{GLL} = 24$.

both in non-homogeneous start-up planar Poiseuille flow and under equilibrium conditions for the same channel geometry. We have proved theoretically in the case of equilibrium that the stress field is anisotropic but divergence-free. The equilibrium results thus generalize those from some earlier work of Brunn and Grisafi [7] for Hookean dumbbells. Numerical results confirm some of our theoretical predictions for the stress field under equilibrium conditions. The results for Poiseuille flow are in very close quantitative agreement with a Brownian dynamics simulation and, for comparable levels of accuracy, are far less CPU expensive. Shear-thinning and bounded intermolecular spring extensibility in the FENE model have been shown, for a given pressure drop, to result in higher flow rates and smaller elastic stresses than in the Hookean case. Our results are in good qualitative agreement with the simulations of Petruccione and Biller [29] for bounded non-homogeneous flow and in particular demonstrate polymer migration to the channel centre away from the bounding walls and the development of steep velocity and stress boundary gradients at the boundaries. Results collapse to those of the usual homogeneous flow FENE model for polymer dimensions sufficiently small compared to the channel wall separation distance.

Finally, whereas we admit that it would be desirable from a micro-mechanical

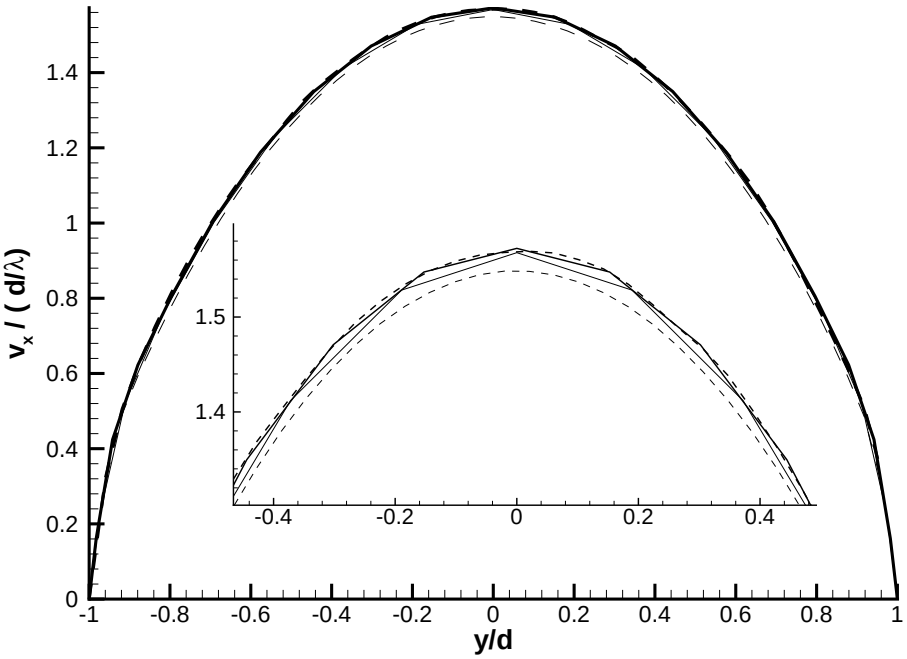

Fig. 12. Velocity computed with the different methods, $l_0/d = 0.1$; dashed thin line – stochastic with $M = 2 \times 10^5$, $N_P = 50$ (CPU time 16 sec), dashed thick line – stochastic with $M = 2 \times 10^6$, $N_P = 50$ (CPU time 1614 sec), solid thin line – deterministic with $N_{GL} = N_{GLL} = 16$ (CPU time 6 sec), solid thick line– deterministic with $N_{GL} = N_{GLL} = 20$ (CPU time 28 sec).

point of view to work with full FENE chains within distances of one polymer length of a solid boundary, the present results should nevertheless be considered to have qualitative value. Full chain simulations are deferred to a follow-up paper.

5 Acknowledgements

The work of the first author has been supported by the Swiss National Science Foundation, grant number 2100-55543. The authors wish to thank one of the referees for a number of insightful remarks which have contributed to their better understanding of the physical significance of what has been presented in this paper.

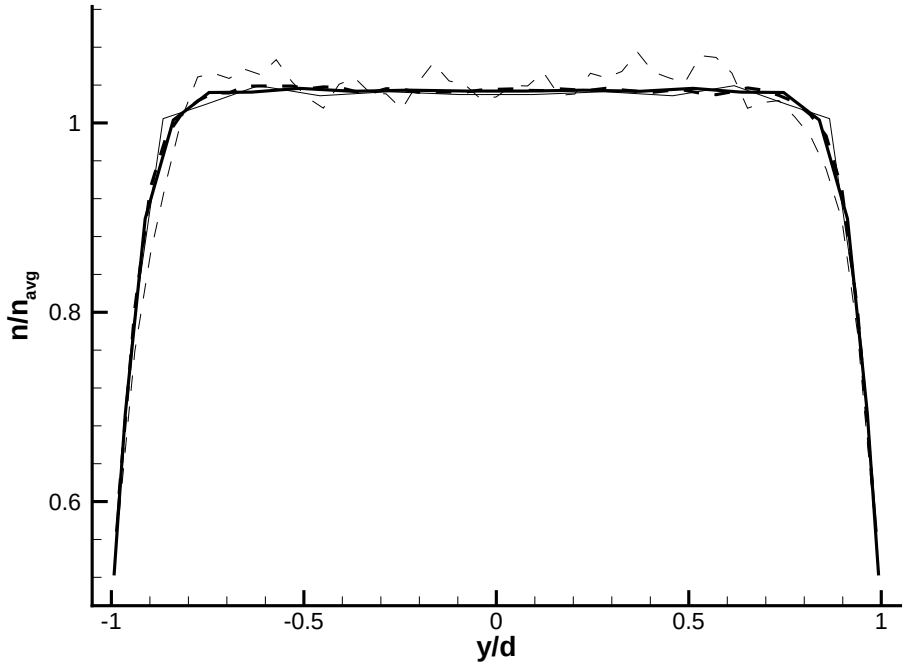

Fig. 13. Polymer number density computed with the different methods, $l_0/d = 0.1$; the meaning of the curves is the same as in Fig. 12. The two thick lines (for stochastic and deterministic methods with finest resolutions) are almost superposed.

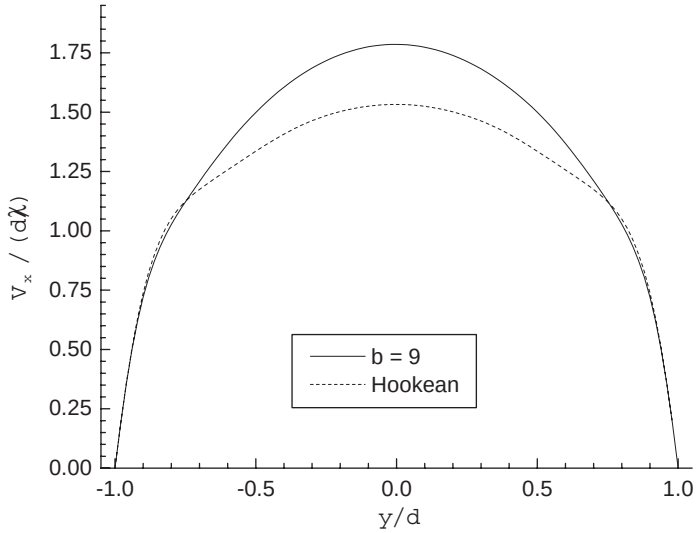

Fig. 14. Comparison of velocity profiles v_x for FENE fluid ($b = 9$) and Oldroyd B fluid ($b = 1 \times 10^6$) computed using the stochastic method with $M = 1 \times 10^5$, $N_P = 101$, $l_0/d = 0.2$, $P^* = 2$.

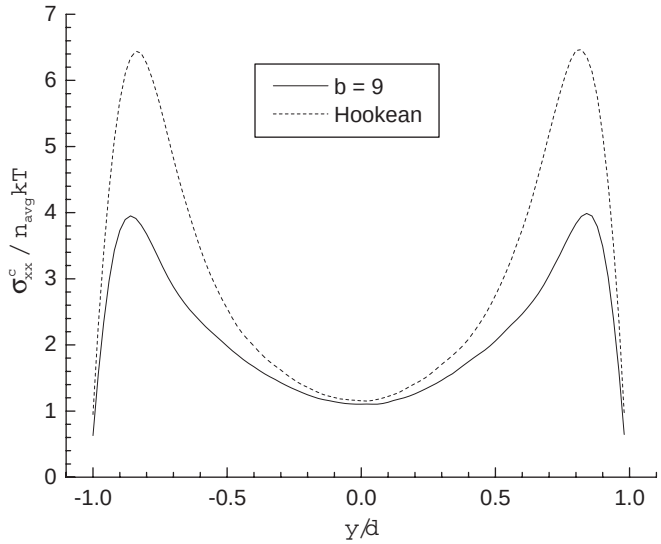

Fig. 15. Comparison of normal stress profiles σ^C_{xx} for FENE fluid ($b = 9$) and Oldroyd B fluid ($b = 1 \times 10^6$) computed using the stochastic method with $M = 1 \times 10^5$, $N_P = 101$, $l_0/d = 0.2$, $P^* = 2$.

A Anisotropy of the stress field in equilibrium

Beginning with (10) in a no-flow situation, we see that the cdf ψ^c_{eq} satisfies

$$\begin{aligned} 0 = &\int_{\mathbf{r}_c}\int_{\Gamma^{\pm}(\mathbf{r}_c)} \left[\left(\frac{2kT}{\zeta}\frac{\partial\psi^c_{eq}}{\partial\mathbf{R}} + \frac{2}{\zeta}\mathbf{F}(\mathbf{R})\psi^c_{eq}\right)\cdot\mathbf{n}\varphi^c\right] dSd\mathbf{r}_c \\ &- \int_{\mathbf{r}_c}\int_{D(\mathbf{r}_c)} \left(\frac{2kT}{\zeta}\frac{\partial\psi^c_{eq}}{\partial\mathbf{R}} + \frac{2}{\zeta}\mathbf{F}(\mathbf{R})\psi^c_{eq}\right)\cdot\frac{\partial\varphi^c}{\partial\mathbf{R}}\, d\mathbf{R}d\mathbf{r}_c \\ &+ \frac{kT}{2\zeta}\int_{\mathbf{r}_c}\int_{D(\mathbf{r}_c)} \frac{\partial^2\psi^c_{eq}}{\partial\mathbf{r}^2}\varphi^c\, d\mathbf{R}d\mathbf{r}_c. \end{aligned} \tag{A.1}$$

This has solution

$$\psi^c_{eq}(\mathbf{r}_c,\mathbf{R}) = \begin{cases} \psi_0(\mathbf{R}), \text{ if } \mathbf{r}_c \pm \mathbf{R}/2 \in \Omega = (-\infty,\infty)\times[-d,d], \\ 0, \text{ otherwise,} \end{cases} \tag{A.2}$$

where

$$\psi_0(\mathbf{R}) = C\left(1 - \frac{|\mathbf{R}|^2}{R^2_{\max}}\right)^{b/2}, \tag{A.3}$$

is the equilibrium cdf for the homogeneous-flow FENE model.

From (14) and (A.2) we may write the spring force contribution to the equilibrium stress tensor as

$$\begin{aligned}\boldsymbol{\sigma}^C_{eq}(\mathbf{r}) &= \int_{|\mathbf{R}|<R_{\max}} \int_{s=\alpha(y,R_y)}^{\beta(y,R_y)} \mathbf{F}(\mathbf{R})\mathbf{R}\psi_0(\mathbf{R})\, ds\, d\mathbf{R}, \\ &= \int_{|\mathbf{R}|<R_{\max}} (\beta(y,R_y)-\alpha(y,R_y))\mathbf{F}(\mathbf{R})\mathbf{R}\psi_0(\mathbf{R})\, d\mathbf{R}, \end{aligned} \tag{A.4}$$

where $\mathbf{r} = (x,y)^T$ and limits α and β on s have been chosen to ensure that $\mathbf{r} + (s-1/2)\mathbf{R} \in \Omega$, i.e. $|y + (s-1/2)R_y| < d$. It is straightforward to show that

$$\beta(y,R_y) - \alpha(y,R_y) = \min\left(1, \left(\frac{d-|y|}{|R_y|}\right)\right). \tag{A.5}$$

Eqn. (A.4) may be rewritten as

$$\boldsymbol{\sigma}^C_{eq} = -kT \int_{|\mathbf{R}|<R_{\max}} (\beta(y,R_y)-\alpha(y,R_y))\mathbf{R}\frac{\partial \psi_0(\mathbf{R})}{\partial \mathbf{R}} d\mathbf{R}, \tag{A.6}$$

and, using integration by parts,

$$\boldsymbol{\sigma}^C_{eq} = kT \int_{|\mathbf{R}|<R_{\max}} \frac{\partial}{\partial \mathbf{R}}((\beta(y,R_y)-\alpha(y,R_y))\mathbf{R})\psi_0(\mathbf{R}) d\mathbf{R}. \tag{A.7}$$

Hence,

$$\begin{aligned}\sigma^C_{eq,xx}(y) &= kT \int_{|\mathbf{R}|<R_{\max}} \frac{\partial}{\partial R_x}\left((\beta(y,R_y)-\alpha(y,R_y))R_x\right)\psi_0(\mathbf{R})\, d\mathbf{R}, \\ &= kT \int_{|\mathbf{R}|<R_{\max}} (\beta(y,R_y)-\alpha(y,R_y))\psi_0(\mathbf{R})\, d\mathbf{R}, \end{aligned} \tag{A.8}$$

and

$$\sigma^C_{eq,yy}(y) = kT \int_{|\mathbf{R}|<R_{\max}} \frac{\partial}{\partial R_y}\left((\beta(y,R_y)-\alpha(y,R_y))R_y\right)\psi_0(\mathbf{R})\, d\mathbf{R}. \tag{A.9}$$

Note that

$$\frac{\partial}{\partial R_y}\left((\beta(y,R_y)-\alpha(y,R_y))R_y\right) = \begin{cases} \frac{\partial R_y}{\partial R_y} = 1, \text{ if } d- \mid y \mid > \mid R_y \mid \\ \frac{\partial}{\partial R_y}\left(\frac{d-|y|}{|R_y|}R_y\right) = 0, \text{ if } d- \mid y \mid < \mid R_y \mid \end{cases}$$

Hence, from (A.9)

$$\sigma^C_{eq,yy}(y) = kT \int_{\{|\mathbf{R}|<R_{\max}\}\bigcap\{|R_y|<d-|y|\}} \psi_0(\mathbf{R})\, d\mathbf{R}, \tag{A.10}$$

and from (A.8) and (A.10) we see that

$$\sigma^C_{eq,xx} - \sigma^C_{eq,yy} = kT \int_{\{|\mathbf{R}|<R_{\max}\}\bigcap\{|R_y|\geq d-|y|\}} \left(\frac{d-|y|}{|R_y|}\right)\psi_0(\mathbf{R})\, d\mathbf{R} \geq 0, \tag{A.11}$$

as stated in Eqn.(22).

As observed in Section 3.1 there is no contradiction between anisotropy in the stress field and equilibrium conditions, since

$$\nabla \cdot \left(\boldsymbol{\sigma}_{eq}^{C} + \boldsymbol{\sigma}_{eq}^{K} \right) = \mathbf{0}. \tag{A.12}$$

The demonstration of this result is in two stages. First, and rather obviously,

$$\sigma_{eq,xy}^{C}(y) = kT \int_{|\mathbf{R}|<R_{\max}} \frac{\partial}{\partial R_x} \left((\beta(y,R_y) - \alpha(y,R_y))R_y \right) \psi_0(\mathbf{R})\, d\mathbf{R} = 0. \tag{A.13}$$

Secondly, the $yy-$component of the total equilibrium Cauchy stress is independent of y. To see this, we introduce the integrals

$$I_1 = \int_{|\mathbf{R}|<R_{\max}} \psi_0(\mathbf{R})\, d\mathbf{R}, \tag{A.14}$$

and

$$I_2 = \int_{\{|\mathbf{R}|<R_{\max}\} \bigcap \{|R_y| \geq d-|y|\}} \psi_0(\mathbf{R})\, d\mathbf{R}. \tag{A.15}$$

Then, we note that the integrand in (16) is non-zero only for $\mathbf{R}$ such that $\mathbf{r} + \mathbf{R} \in \Omega$, i.e. $y + R_y \in (-d, d)$. Hence, we obtain in the case $y > 0$, for example, that

$$\sigma_{eq,yy}^{K} = -2kTn(y) = -2kT \int_{\{|\mathbf{R}|<R_{\max}\} \bigcap \{R_y < d-y\}} \psi_0(\mathbf{R})\, d\mathbf{R}, \tag{A.16}$$

or, by the symmetry of $\psi_0(\mathbf{R})$,

$$\sigma_{eq,yy}^{K} = -2kT(I_1 - I_2/2).$$

Thus, we can use (A.10) to obtain

$$\begin{aligned} \sigma_{yy}^{C} + \sigma_{yy}^{K} &= kT(I_1 - I_2) - 2kT(I_1 - I_2/2) \\ &= -kTI_1, \end{aligned} \tag{A.17}$$

and this is independent of y.

References

[1] M. V. Apostolakis, V. G. Mavrantzas and A. N. Beris, Stress gradient-induced migration effects in the Taylor-Couette flow of a dilute polymer solution, J. Non-Newtonian Fluid Mech., 102 (2002) 409-445.

[2] R. C. Armstrong, R. Nayak, I. Ghosh and R. A. Brown, The use of kinetic theory and microstructural models in the analysis of complex flows of viscoelastic liquids, In *Proceedings of the 12th International Congress on Rheology*, Laval University, Québec, Aug. 18-23, 1996, edited by Aït-Kadi, A., J. M. Dealy, D. F. James and M. C. Williams.

[3] A. N. Beris and V. G. Mavrantzas, On the compatibility between various macroscopic formalisms for the concentration and flow of dilute polymer solutions, J. Rheol., 38 (1994) 1235-1250.

[4] A. V. Bhave, R. C. Armstrong and R. A. Brown, Kinetic theory and rheology of dilute, nonhomogeneous polymer solutions, J. Chem. Phys., 95 (1991) 2988-3000.

[5] P. Biller and F. Petruccione, The flow of dilute polymer solutions in confined geometries: A consistent numerical approach, J. Non-Newtonian Fluid Mech., 25 (1987) 347-364.

[6] R. B. Bird, C. F. Curtiss, R. C. Armstrong and O. Hassager, Dynamics of Polymeric Liquids, Vol. 2, (John Wiley & Sons, New York, 1987).

[7] P. O. Brunn and S. Grisafi, Kinetic theory of a dilute polymer solution in a small channel: equilibrium results, Chem. Eng. Commun., 36 (1985) 367-383.

[8] C. Chauvière, J. Fang, A. Lozinski and R. G. Owens, On the numerical simulation of flows of polymer solutions using high-order methods based based on the Fokker-Planck equation, Int. J. Mod. Phys. B, 17 (2003) 9-14.

[9] C. Chauvière and A. Lozinski, Simulation of dilute polymer solutions using a Fokker-Planck equation, Computers and Fluids, 33 (2003) 687-696.

[10] C. F. Curtiss and R. B. Bird, Diffusion-stress relations in polymer mixtures, J. Chem. Phys., 111 (1999) 10362-10370.

[11] A. W. El-Kareh and L. G. Leal, Existence of solutions for all Deborah numbers for a non-Newtonian model modified to include diffusion, J. Non-Newtonian Fluid Mech., 33 (1989) 257-287.

[12] X. Fan, Molecular model and flow calculation: I. The numerical solutions to multibead-rod models in homogeneous flows, Acta Mech. Sin., 5 (1989) 49-59.

[13] X. Fan, Molecular models and flow calculations: II. Simulation of steady planar flow, Acta Mech. Sin., 5 (1989) 216-226.

[14] X.-J. Fan, Viscosity, first normal-stress coefficient, and molecular stretching in dilute polymer solutions, J. Non-Newtonian Fluid Mech., 17 (1985) 125-144.

[15] X.-J. Fan, Viscosity, first normal-stress coefficients and molecular stretching in concentrated solutions and melts, J. Non-Newtonian Fluid Mech., 17 (1985) 251-265.

[16] X.-J. Fan, A numerical investigation of the hydrodynamic interaction for Hookean dumbbell suspensions in steady state shear flow, J. Chem. Phys., 85 (1985) 6237-6238.

[17] J. Fang, M. Kröger and H. C. Öttinger, A thermodynamically admissible reptation model for fast flows of entangled polymers. II. Model predictions for shear and extensional flows, J. Rheol., 44 (2000) 1293–1317.

[18] M. A. Hulsen, A. P. G. van Heel and B. H. A. A. van den Brule, Simulation of viscoelastic flows using Brownian configuration fields, J. Non-Newtonian Fluid Mech., 70 (1997) 79-101.

[19] A. Lozinski and C. Chauvière, A fast solver for Fokker-Planck equation applied to viscoelastic flows calculations: 2D FENE model, J. Comp. Phys., 189 (2003) 607-625.

[20] A. Lozinski, C. Chauvière, J. Fang and R. G. Owens, Fokker-Planck simulations of fast flows of melts and concentrated polymer solutions in complex geometries, J. Rheol., 47 (2003) 535-561.

[21] V. G. Mavrantzas and A. N. Beris, Modeling the rheology and flow-induced concentration changes in polymer solutions, Phys. Rev. Lett., 69 (1992) 273-276; 70 (1993) 2659.

[22] V. G. Mavrantzas and A. N. Beris, Theoretical study of wall effects on the rheology of dilute polymer solutions, J. Rheol., 36 (1992) 175-213.

[23] V. G. Mavrantzas, A. Souvaliotis and A. N. Beris, Pseudo-spectral calculations of stress-induced concentration changes in viscometric flows of polymer solutions, Theor. Comp. Fluid Dynam. 5 (1993) 3-31.

[24] R. Nayak, Molecular simulation of liquid crystal polymer flow: a wavelet-finite element analysis, PhD thesis, MIT, Cambridge, MA. (1998).

[25] H. C. Öttinger, Incorporation of polymer diffusivity and migration into constitutive equations, Rheol. Acta, 31 (1992) 14-21.

[26] H. C. Öttinger, A thermodynamically admissible reptation model for fast flows of entangled polymers, J. Rheol., 43 (1999) 1461-1493.

[27] H. C. Öttinger, B. H. A. A. van den Brule and M. A. Hulsen, Brownian configuration fields and variance reduced CONNFFESSIT, J. Non-Newtonian Fluid Mech., 70 (1997) 255-261.

[28] R. G. Owens and T. N. Phillips, Computational Rheology, Imperial College Press/World Scientific, London, 2002.

[29] F. Petruccione and P. Biller, A consistent numerical analysis of the tube flow of dilute polymer solutions, J. Rheol., 32 (1988) 1-21.

[30] J. K. C. Suen, Y. L. Joo and R. C. Armstrong, Molecular orientation effects in viscoelasticity, Annu. Rev. Fluid Mech., 34 (2002) 417-444.

[31] R. Sureshkumar and A. N. Beris, Effect of artificial stress diffusivity on the stability of numerical calculations and the flow dynamics of time-dependent viscoelastic flows, J. Non-Newtonian Fluid Mech., 60 (1995) 53–80.

[32] H. R. Warner, Kinetic theory and rheology of dilute suspensions of finitely extendible dumbbells, Ind. Eng. Chem. Fundam., 11 (1972) 379-387.